**Article:**
Hussein, MS and Lesnic, D (2015) Identification of the time-dependent conductivity of an inhomogeneous diffusive material. Applied Mathematics and Computation, 269. 35 - 58. ISSN 0096-3003

https://doi.org/10.1016/j.amc.2015.07.039

# Identification of the Time-Dependent Conductivity of an Inhomogeneous Diffusive Material

M.S. Hussein[1,2] and D. Lesnic[1]
[1]*Department of Applied Mathematics, University of Leeds, Leeds LS2 9JT, UK*
[2]*Department of Mathematics, College of Science, University of Baghdad, Baghdad, Iraq*
E-mails: mmmsh@leeds.ac.uk (M.S. Hussein), amt5ld@maths.leeds.ac.uk (D. Lesnic).

**Abstract**
In this paper, we consider a couple of inverse problems of determining the time-dependent thermal/hydraulic conductivity from Cauchy data in the one-dimensional heat/diffusion equation with space-dependent heat capacity/ specific storage. The well-posedness of these inverse problems in suitable spaces of continuously differentiable functions are studied. For the numerical realisation, the problems are discretised using the finite-difference method and recast as nonlinear least-squares minimization problems with a simple positivity lower bound on the unknown thermal/ hydraulic conductivity. Numerically, this is effectively solved using the *lsqnonlin* routine from the MATLAB toolbox. Regularization is included wherever necessary. Numerical results are presented and discussed for several benchmark test examples showing that accurate and stable numerical solutions are achieved. The outcomes of this study will be relevant and of importance to the applied mathematics inverse problems community working on thermal/hydraulic property determination in heat transfer and porous media.

**Keywords:** Inverse problem; Finite-difference method; Thermal/hydraulic conductivity; Nonlinear optimization.

# 1 Introduction

The scope of inverse problems has existed in various branches of physics, engineering and mathematics for a long time. The theory of inverse problems has been extensively developed within the past decade due partly to its importance in applications; on the other hand the numerical solutions to such problems need huge computations and also reliable numerical methods. For instance, deconvolution in seismic exploration, image reconstruction and parameter identification all require high performance computers and reliable solution methods to carry out the computation [17].

Parameter identification problems consist in using the input of actual observation or indirect measurement contaminated with noise, to infer the values of the parameters characterizing the system under investigation. Often, these inverse problems are ill-posed according to the Hadamard concept which is: if the solution does not exist or, is not unique or, if it violates the continuous dependence upon input data. Most identification problems satisfy the first two conditions and violate the third one which is the stability.

Inverse coefficient identification problems have been the point of interest to many significant researchers in recent years. Determination of leading coefficient or, the coefficient of highest-order derivative in the parabolic heat equation has been investigated widely and in many practical applications. For example, in [6] the problem of space-dependent diffu-

sivity identification has been studied, while the time-dependent case has been investigated in [14]. Also, for the temperature-dependent case we refer to [2, 18].

In this paper, we consider obtaining the numerical solution of inverse time-dependent multiplier of the highest-order derivative in the parabolic heat equation. Physically, in heat transfer this unknown thermal property coefficient corresponds to the thermal conductivity of an inhomogeneous heat conductor which has a space-varying known heat capacity. It is this later physically realistic feature that makes some of the methods of previous studies [3, 9, 10, 19] of time-dependent thermal diffusivity identification inapplicable. The same problem can be formulated in porous media by replacing the thermal properties with the corresponding hydraulic ones.

With respect to what boundary conditions are specified and what additional measurements are performed, the mathematical formulations of two inverse problems are given in Section 2. In that section, we also recall the previous unique solvability results of [13, Section 4.3]. Furthermore, new stability theorems are stated and proved. Moreover, since obtaining the solution of these problems has never been attempted before it is therefore, the purpose of our study to undertake such a numerical investigation. Consequently, a numerical method based on the Crank-Nicholson finite-difference scheme is employed as direct solver in a nonlinear least-squares minimization, as described in Sections 3 and 4, respectively. This combination yields accurate and stable numerical solutions, as it will be discussed in Section 5. Finally, the conclusions of this research and possible future work are highlighted in Section 6.

# 2 Mathematical Formulation

Let $L > 0$ and $T > 0$ be fixed numbers and consider the inverse problem of finding the time-dependent thermal conductivity $C[0,T] \ni a(t) > 0$ for $t \in [0,T]$, and the temperature $u(x,t) \in C^{2,1}(Q_T) \cap C^{1,0}(\overline{Q}_T)$, which satisfy the heat equation

$$c(x)\frac{\partial u}{\partial t}(x,t) = a(t)\frac{\partial^2 u}{\partial x^2}(x,t) + F(x,t), \qquad (x,t) \in Q_T := (0,L) \times (0,T), \tag{1}$$

where $c(x) > 0$ is the heat capacity and $F$ is a heat source, the initial condition

$$u(x,0) = \phi(x), \qquad x \in [0,L], \tag{2}$$

the Dirichlet boundary conditions

$$u(0,t) = \mu_1(t), \qquad u(L,t) = \mu_2(t), \qquad t \in [0,T], \tag{3}$$

and the heat flux additional measurement

$$-a(t)u_x(0,t) = \mu_3(t), \qquad t \in [0,T]. \tag{4}$$

Dividing equation (1) by $c(x)$ and denoting

$$b(x) = \frac{1}{c(x)}, \quad f(x,t) = \frac{F(x,t)}{c(x)} \tag{5}$$

we obtain

$$\frac{\partial u}{\partial t}(x,t) = a(t)b(x)\frac{\partial^2 u}{\partial x^2}(x,t) + f(x,t), \qquad (x,t) \in Q_T. \tag{6}$$

## 2.1 Inverse Problem I

The above inverse problem (termed Inverse Problem I) was previously investigated theoretically in Section 4.3 of [13] where its unique solvability has been established, as follows.

**Theorem 1.** (Existence of solution of Inverse Problem I)
*Suppose that the following conditions hold:*

1. *(regularity conditions)* $b \in C^1[0,L]$, $\phi \in C^1[0,L]$, $\mu_i \in C^1[0,T]$ *for* $i = 1,2$, $\mu_3 \in C[0,T]$, $f \in C^{1,0}(\overline{Q}_T)$;
2. *(compatibility conditions)* $\phi(0) = \mu_1(0)$, $\phi(L) = \mu_2(0)$.
3. *(non-vanishing and monotonicity conditions)* $\phi'(x) > 0$, $b(x) > 0$, $b'(x) \leq 0$ *for* $x \in [0,L]$, $\mu_3(t) < 0$, $\mu_1'(t) - f(0,t) \leq 0$, $\mu_2'(t) - f(L,t) \geq 0$ *for* $t \in [0,T]$, $f_x(x,t) \geq 0$ *for* $(x,t) \in \overline{Q}_T$;

*Then there exists a solution to the inverse problem (2)–(4) and (6).*

**Theorem 2.** (Uniqueness of solution of Inverse Problem I)
*If* $b \in C^1[0,L]$, $b(x) > 0$ *for* $x \in [0,L]$, $\mu_3(t) \neq 0$ *for* $t \in [0,T]$, *then the solution of the inverse problem (2)–(4) and (6) is unique.*

Lower-order terms, e.g. $c_1(x,t)u_x + c_2(x,t)u$, with known functions $c_1$ and $c_2$ can also be added to the right-hand-side of equation (6) to model convection and reaction.

Next, we address the stability of solution.

**Theorem 3.** (Local stability of solution of Inverse Problem I)
*Suppose that the conditions of Theorem 1 are satisfied. Let* $\mu_3$ *and* $\tilde{\mu}_3$ *be two data in (4) and let* $(a(t), u(x,t))$ *and* $(\tilde{a}(t), \tilde{u}(x,t))$ *be the corresponding solutions of the inverse problem (2)–(4) and (6). Then, for sufficiently small* $T$, *the following local stability estimate holds:*

$$\|a - \tilde{a}\|_{C[0,T]} \leq C\|\mu_3 - \tilde{\mu}_3\|_{C[0,T]}, \tag{7}$$

*for some positive constant* $C$.

*Proof:* We observe first that the pair of differences $A(t) = a(t) - \tilde{a}(t)$, $U(x,t) = u(x,t) - \tilde{u}(x,t)$ is a solution of the following inverse problem:

$$U_t = a(t)b(x)U_{xx} + A(t)b(x)\tilde{u}_{xx}, \quad (x,t) \in Q_T, \tag{8}$$

$$U(x,0) = 0, \quad x \in [0,L], \tag{9}$$

$$U(0,t) = U(L,t) = 0, \quad t \in [0,T], \tag{10}$$

$$-a(t)U_x(0,t) = A(t)\tilde{u}_x(0,t) + \mu_3(t) - \tilde{\mu}_3(t), \quad t \in [0,T]. \tag{11}$$

The function $U(x,t)$ satisfying (8)–(10) can be expressed with the aid of its Green's function $G_1$ as

$$U(x,t) = \int_0^t \int_0^L G_1(x,t;\xi,\tau)A(\tau)b(\xi)\tilde{u}_{\xi\xi}(\xi,\tau)d\xi d\tau, \quad (x,t) \in Q_T. \tag{12}$$

Differentiating (12) with respect to $x$ and substituting into (11), one obtains

$$-a(t)\int_0^t A(\tau)\left(\int_0^L G_{1x}(0,t;\xi,\tau)b(\xi)\tilde{u}_{\xi\xi}(\xi,\tau)d\xi\right)d\tau = A(t)\tilde{u}_x(0,t)+\mu_3(t)-\tilde{\mu}_3(t), \quad t\in[0,T]. \tag{13}$$

Since $\tilde{\mu}_3(t)\neq 0$, from (4) we have that $\tilde{u}_x(0,t)\neq 0$ for $t\in[0,T]$. This means that (13) is a linear Volterra integral equation of the second kind in $A(t)$ written in the form

$$A(t) = g(t)+\int_0^t H(t,\tau)A(\tau)d\tau, \quad t\in[0,T], \tag{14}$$

where

$$g(t) := \frac{\tilde{\mu}_3(t)-\mu_3(t)}{\tilde{u}_x(0,t)} \qquad t\in[0,T], \tag{15}$$

is a continuous function and the kernel

$$H(t,\tau) := -\frac{a(t)}{\tilde{u}_x(0,t)}\int_0^L G_{1x}(0,t;\xi,\tau)b(\xi)\tilde{u}_{\xi\xi}(\xi,\tau)d\xi \tag{16}$$

has a weak integrable singularity. This follows from the estimates of [13, p.147], where we have that there exists a positive constant $C_1$ such that

$$\left|G_{1x}(0,t,\xi,\tau)\right| \leq \frac{C_1}{\theta(t)-\theta(\tau)}\sum_{n=-\infty}^{\infty}\exp\left(-\frac{(\beta(\xi)+2n\beta(L))^2}{8(\theta(t)-\theta(\tau))}\right), \quad t>\tau, \tag{17}$$

which upon integration yields

$$\int_0^L \left|G_{1x}(0,t,\xi,\tau)\right|d\xi \leq \frac{C_2}{\sqrt{\theta(t)-\theta(\tau)}}, \quad t>\tau, \tag{18}$$

for some positive constant $C_2$. In (17), we used the notations

$$\theta(t) = \int_0^t a(\tau)d\tau, \quad \beta(x) = \int_0^x \frac{d\xi}{\sqrt{b(\xi)}}. \tag{19}$$

Note that $\theta\in C^1[0,T]$ is a strictly increasing function with $\theta(0)=0$ and $\theta'(t)=a(t)>0$ for $t\in[0,T]$. For convenience, let us deduce from (18) that

$$\int_0^L \left|G_{1x}(0,t,\xi,\tau)\right|d\xi \leq \frac{C_2}{\min_{\rho\in[0,T]}a(\rho)}\frac{a(\tau)}{\sqrt{\theta(t)-\theta(\tau)}}, \quad t>\tau, \tag{20}$$

which when used into (16) integrated produces the inequality

$$\int_0^t \left|H(t,\tau)\right|d\tau \leq C_3\int_0^t \frac{a(\tau)}{\sqrt{\theta(t)-\theta(\tau)}}d\tau = 2C_3\sqrt{\theta(t)}, \tag{21}$$

for some positive constant $C_3$. Now since the function $\sqrt{\theta(t)}$ is a monotonically increasing function and $\lim_{t\to 0}\sqrt{\theta(t)}=0$, according to standard theory of linear Volterra integral

equations of the second kind, see e.g. [1, Section 8.2], it follows that equation (14) is uniquely solvable. Furthermore, from (14) and (21) it follows that

$$\begin{aligned}\big|A(t)\big| &\le \|g\|_{C[0,T]} + \int_0^t \big|H(t,\tau)\big|\big|A(\tau)\big|d\tau \\ &\le \|g\|_{C[0,T]} + 2C_3\sqrt{\theta(T)}\|A\|_{C[0,T]}, \quad t \in [0,T]. \end{aligned} \tag{22}$$

Since $\theta(0) = 0$ and $\theta$ is a monotonically increasing function, then, for sufficiently small $T$ we have that $1 > 2C_3\sqrt{\theta(T)}$. Then, (15) and (22) yield that the stability estimate (7) holds, where we have used that from (15),

$$\|g\|_{C[0,T]} \le \frac{\|\tilde{\mu}_3(t) - \mu_3(t)\|_{C[0,T]}}{\min_{t\in[0,T]} |\tilde{u}_x(0,t)|}. \tag{23}$$

A similar local stability can be obtained from (12) and (7) for the norm of the temperature difference $\|U\|_{C(\overline{Q}_T)} = \|u - \tilde{u}\|_{C(\overline{Q}_T)}$.

Altogether, we have established that under the assumptions of Theorem 1, the solution $(a(t), u(x,t))$ locally depends continuously upon the input data (4) in the maximum norm of $C[0,T]$.

Later on, in the numerical results of Section 5.1, the well-posedness of the Inverse Problem I established in Theorems 1–3 will be highlighted through the fact that no regularization is needed for obtaining a stable and accurate numerical solution.

## 2.2 Inverse Problem II

For completeness, we also investigate another related inverse problem (termed Inverse Problem II) which requires the determination of the thermal conductivity $C[0,T] \ni a(t) > 0$ for $t \in [0,T]$ and the temperature $u(x,t) \in C^{2,1}(\overline{Q}_T)$, which satisfy the heat equation (6), the initial condition (2), the Neumann boundary conditions

$$-u_x(0,t) = \nu_1(t), \qquad u_x(L,t) = \nu_2(t), \qquad t \in [0,T], \tag{24}$$

and the boundary temperature additional measurement

$$u(0,t) = \mu_1(t), \qquad t \in [0,T]. \tag{25}$$

This inverse problem was also previously investigated in Section 4.3 of [13], where its unique solvability has been established, as follows.

**Theorem 4.** (Existence of solution of Inverse Problem II)
*Suppose that the following conditions hold:*

1. $b \in C^2[0,L]$, $\phi \in C^2[0,L]$, $\nu_i \in C^1[0,T]$, $i = 1,2$, $\mu_1 \in C^1[0,T]$, $f \in C^{1,0}(\overline{Q}_T)$;
2. $b(x) > 0$, $\phi'(x) \ge 0$, $(\phi'(x)\sqrt{b(x)})' > 0$, $b'(x) \le 0$, $b''(x) \le 0$ *for* $x \in [0,L]$; $\nu_1(t) \le 0$, $\nu_2(t) \ge 0$, $\mu_1'(t) - f(0,t) > 0$, $f_x(0,t) + \mu_1'(t) \ge 0$, $\nu_2'(t) - f_x(L,t) \ge 0$ *for* $t \in [0,T]$; $f_x(x,t) \ge 0$, $(f_x(x,t)\sqrt{b(x)})_x \ge 0$ *for* $(x,t) \in \overline{Q}_T$;
3. $\phi'(0) = -\nu_1(0)$, $\phi'(L) = \nu_2(0)$, $\phi(0) = \mu_1(0)$.

*Then there exists a solution to the inverse problem (2), (6), (24) and (25).*

**Theorem 5.** (Uniqueness of solution of Inverse Problem II)
*If $b \in C^1[0,L]$, $b(x) > 0$ for $x \in [0,L]$, $\mu_1'(t) - f(0,t) \neq 0$ for $t \in [0,T]$, then the solution of the inverse problem (2), (6), (24) and (25) is unique.*

**Theorem 6.** (Local stability of solution of Inverse Problem II)
*Suppose that the conditions of Theorem 4 are satisfied. Let $\mu_1$ and $\tilde{\mu}_1$ be two data in (25) and let $(a(t), u(x,t))$ and $(\tilde{a}(t), \tilde{u}(x,t))$ be the corresponding solutions of the inverse problem (2), (6), (24) and (25). Then for sufficiently small $T$, the following local stability estimate holds:*

$$\|a - \tilde{a}\|_{C[0,T]} \leq C\|\mu_1 - \tilde{\mu}_1\|_{C^1[0,T]}, \tag{26}$$

*for some positive constant $C$.*

*Proof:* As in the proof of Theorem 3, first observe that the pair of differences $(A(t), U(x,t))$ is a solution to the problem given by equations (6), (25),

$$-U_x(0,t) = U_x(L,t) = 0, \quad t \in [0,T], \tag{27}$$
$$U(0,t) = \mu_1(t) - \tilde{\mu}_1(t), \quad t \in [0,T]. \tag{28}$$

Write the solution of the problem (6), (25), and (27) with the aid of its Green's function $G_2$ as

$$U(x,t) = \int_0^t \int_0^L G_2(x,t;\xi,\tau)A(\tau)b(\xi)\tilde{u}_{\xi\xi}(\xi,\tau)d\xi d\tau, \quad (x,t) \in Q_T. \tag{29}$$

Differentiating condition (28) with $t$ and using equation (25) at $x = 0$, we obtain

$$\begin{aligned} A(t)b(0)\tilde{u}_{xx}(0,t) + a(t)b(0)\int_0^t A(\tau)\left(\int_0^L G_{2xx}(0,t;\xi,\tau)b(\xi)\tilde{u}_{\xi\xi}(\xi,\tau)d\xi\right)d\tau \\ = \mu_1'(t) - \tilde{\mu}_1'(t), \quad t \in [0,T]. \end{aligned} \tag{30}$$

Since $\tilde{u}(x,t)$ satisfies equations (6) and (25) we obtain

$$\tilde{a}(t)b(0)\tilde{u}_{xx}(0,t) = \mu_1'(t) - f(0,t) \neq 0, \quad t \in [0,T] \tag{31}$$

This means that (30) is a linear Volttera integral equation of the second kind in $A$ written in the form

$$A(t) = h(t) + \int_0^t Q(t,\tau)A(\tau)d\tau, \quad t \in [0,T], \tag{32}$$

where

$$h(t) := \frac{(\mu_1'(t) - \tilde{\mu}_1'(t))\tilde{a}(t)}{\mu_1'(t) - f(0,t)}, \quad t \in [0,T], \tag{33}$$

is a continuous function and the kernel

$$Q(t,\tau) := -\frac{a(t)}{\tilde{u}_{xx}(0,t)}\int_0^L G_{2xx}(0,t;\xi,\tau)b(\xi)\tilde{u}_{\xi\xi}(\xi,\tau)d\xi \tag{34}$$

has an integrable singularity, see [13, pp. 66-67]. Therefore, (32) is uniquely solvable. Furthermore,

$$\begin{aligned}\big|A(t)\big| &\leq \|h\|_{C[0,T]} + \int_0^t \big|Q(t,\tau)\big|\big|A(\tau)\big|d\tau \\ &\leq \|h\|_{C[0,T]} + C_3(T)\|A\|_{C[0,T]}, \quad t \in [0,T],\end{aligned} \tag{35}$$

where $C_3(t) := \int_0^t |Q(t,\tau)|d\tau$. Clearly since $C_3 \geq 0$ and $C_3(0) = 0$, for sufficiently small $T$ we can have $C_3(T) < 1$. Remark also that from (32)

$$\big\|h\big\|_{C[0,T]} \leq C_4\|\mu_1 - \tilde{\mu}_1\|_{C^1[0,T]}. \tag{36}$$

Then (35) and (36) yield the local stability estimate (26). This concludes the proof of Theorem 6.

Note that unlike Inverse Problem I, in the Inverse Problem II, the estimate (26) involves the derivatives of the noisy functions $\mu_1$ and $\tilde{\mu}_1$ which in itself is an unstable procedure which needs to be regularized.

We finally mention that another related inverse formulation given by equations (2), (3), (6) and the additional measurement

$$-u_x(0,t) = \nu_1(t), \quad t \in [0,T] \tag{37}$$

has been investigated in [11]. The choice of additional measurements (4), or (25), or (37), is important for the inverse problem formulation, as it contains the richness of the information supplied in order to retrieve more effectively the unknown time-dependent conductivity.

# 3 Solution of Direct Problems

## 3.1 The Dirichlet direct problem

In this section, we consider the direct (the inverse of the Inverse Problem I) initial Dirichlet boundary value problem given by equations (2), (3) and (6), where $a(t)$, $b(x)$, $f(x,t)$, $\phi(x)$ and $\mu_i(t)$, $i = 1, 2$, are known and the temperature $u(x,t)$ is the solution to be determined. We use the finite-difference method (FDM) with a Crank-Nicholson scheme [15], which is unconditionally stable and second-order accurate in space and time.

The discrete form of the direct problem (2), (3) and (6) is as follows. We subdivide the domain $Q_T = (0,L)\times(0,T)$ into $M \times N$ subintervals of equal step length $\Delta x = L/M$ and $\Delta t = T/N$. At the node $(i,j)$ we denote $u_{i,j} = u(x_i,t_j)$, $a(t_j) = a_j$, $b(x_i) = b_i$ and $f(x_i,t_j) = f_{i,j}$, where $x_i = i\Delta x$, $t_j = j\Delta t$ for $i = \overline{0,M}$, $j = \overline{0,N}$.

The Crank-Nicolson FDM for the general partial differential equation

$$u_t = G(x,t,u_{xx}) \tag{38}$$

is

$$\frac{u_{i,j+1} - u_{i,j}}{\Delta t} = \frac{1}{2}\left(G_{i,j} + G_{i,j+1}\right), \qquad i = \overline{1,(M-1)},\ j = \overline{0,(N-1)}. \tag{39}$$

where

$$G_{i,j} = G\left(x_i, t_j, \frac{u_{i+1,j} - 2u_{i,j} + u_{i-1,j}}{(\Delta x)^2}\right), \quad i = \overline{1,(M-1)},\ j = \overline{0,(N-1)}. \tag{40}$$

Equation (39) has to be solved subject to the discretised form of equations (2) and (3), namely,

$$u_{i,0} = \phi(x_i), \qquad i = \overline{0,M}, \tag{41}$$

$$u_{0,j} = \mu_1(t_j), \qquad u_{M,j} = \mu_2(t_j), \qquad j = \overline{0,N}. \tag{42}$$

For our problem, equation (1) can be discretised in the form of (39) as

$$\begin{aligned} &- C_{i,j+1}u_{i-1,j+1} + (1 + B_{i,j+1})u_{i,j+1} - C_{i,j+1}u_{i+1,j+1} \\ &\qquad = C_{i,j}u_{i-1,j} + (1 - B_{i,j})u_{i,j} + C_{i,j}u_{i+1,j} + \frac{\Delta t}{2}\left(f_{i,j} + f_{i,j+1}\right) \end{aligned} \tag{43}$$

for $i = \overline{1,(M-1)}$, $j = \overline{0,(N-1)}$, where

$$C_{i,j} = \frac{(\Delta t)a_j b_i}{2(\Delta x)^2}, \qquad B_{i,j} = \frac{(\Delta t)a_j b_i}{(\Delta x)^2}.$$

At each time step $t_{j+1}$ for $j = \overline{0,(N-1)}$, using the Dirichlet boundary conditions (42), the difference equation (43) can be reformulated as a $(M-1)\times(M-1)$ system of linear equations of the form,

$$D\mathbf{u}_{j+1} = E\mathbf{u}_j + \mathbf{b}, \tag{44}$$

where

$$\mathbf{u}_{j+1} = (u_{1,j+1}, u_{2,j+1}, ..., u_{M-1,j+1})^{tr},$$

$$D = \begin{pmatrix} 1+B_{1,j+1} & -C_{1,j+1} & 0 & \cdots & 0 & 0 & 0 \\ -C_{2,j+1} & 1+B_{2,j+1} & -C_{2,j+1} & \cdots & 0 & 0 & 0 \\ \vdots & \vdots & \vdots & \ddots & \vdots & \vdots & \vdots \\ 0 & 0 & 0 & \cdots & -C_{M-2,j+1} & 1+B_{M-2,j+1} & -C_{M-2,j+1} \\ 0 & 0 & 0 & \cdots & 0 & -C_{M-1,j+1} & 1+B_{M-1,j+1} \end{pmatrix},$$

$$E = \begin{pmatrix} 1-B_{1,j} & C_{1,j} & 0 & \cdots & 0 & 0 & 0 \\ C_{2,j} & 1-B_{2,j} & C_{2,j} & \cdots & 0 & 0 & 0 \\ \vdots & \vdots & \vdots & \ddots & \vdots & \vdots & \vdots \\ 0 & 0 & 0 & \cdots & C_{M-2,j} & 1-B_{M-2,j} & C_{M-2,j} \\ 0 & 0 & 0 & \cdots & 0 & C_{M-1,j} & 1-B_{M-1,j} \end{pmatrix},$$

and

$$\mathbf{b} = \begin{pmatrix} \frac{\Delta t}{2}(f_{1,j} + f_{1,j+1}) + C_{1,j+1}\mu_1(t_j) \\ \frac{\Delta t}{2}(f_{2,j} + f_{2,j+1}) \\ \vdots \\ \frac{\Delta t}{2}(f_{M-2,j} + f_{M-2,j+1}) \\ \frac{\Delta t}{2}(f_{M-1,j} + f_{M-1,j+1}) + C_{M-1,j+1}\mu_2(t_j) \end{pmatrix}.$$

### 3.1.1 Example

As an example, consider the direct problem (2), (3) and (6) with $T = L = 1$ and

$$\begin{aligned} a(t) &= 1 + t, \quad b(x) = 2 - x^2, \quad \phi(x) = u(x,0) = x + \sin(x), \\ \mu_1(t) &= u(0,t) = 8t, \quad \mu_2(t) = u(1,t) = 1 + \sin(1) + 8t, \\ f(x,t) &= 8 + (1+t)(2-x^2)\sin(x). \end{aligned}$$

The exact solution is given by

$$u(x,t) = x + \sin(x) + 8t \tag{45}$$

and the desired heat flux output (4) is

$$\mu_3(t) = -a(t)u_x(0,t) = -2 - 2t. \tag{46}$$

The numerical and exact solutions for the temperature $u(x,t)$ at interior points are shown in Figure 1 and one can observe that an excellent agreement is obtained. Figure 2 shows the numerical solution in comparison with the exact one for $\mu_3(t)$ and the curves look indistinguishable. The $x$-partial derivative of $u(x,t)$ at $x = 0$ has been evaluated using the following $O(h^2)$ finite-difference approximation formula:

$$u_x(0,t_j) = \frac{4u_{1,j} - u_{2,j} - 3u_{0,j}}{2(\Delta x)}, \qquad j = \overline{0,N}. \tag{47}$$

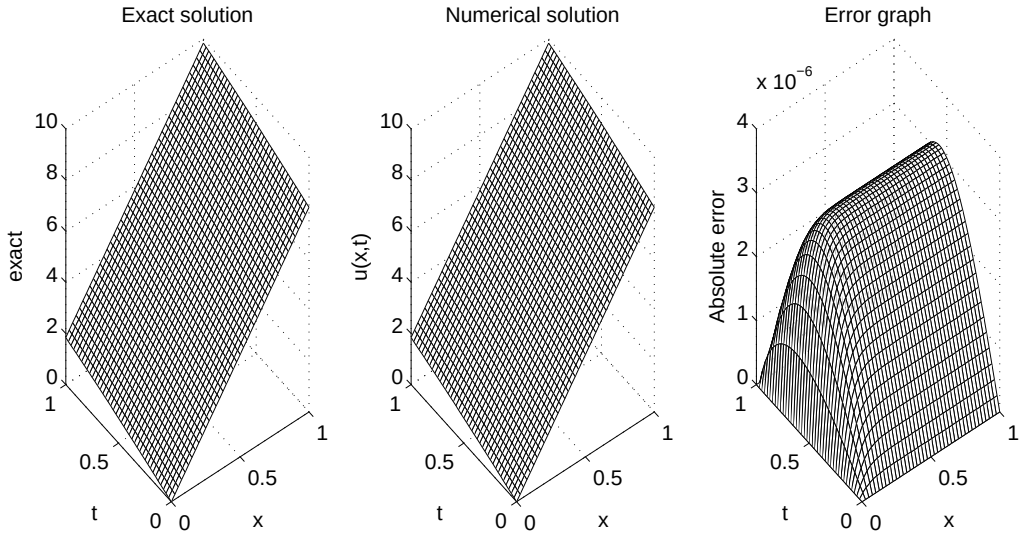


Figure 1: Exact and numerical solutions for the temperature $u(x,t)$ and the absolute error for the Dirichlet direct problem obtained with $M = N = 40$.

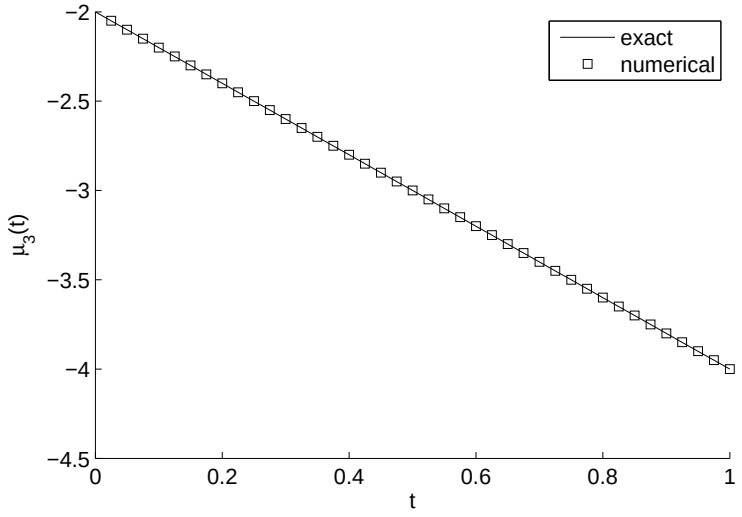


Figure 2: Exact and numerical solutions for the heat flux $\mu_3(t)$ of the Dirichlet direct problem obtained with $M = N = 40$.

## 3.2 The Neumann direct problem

The FDM analysis for the direct (the inverse of the Inverse Problem II) initial Neumann boundary value problem given by equations (2), (6) and (24) is similar to that of direct Dirichlet problem of previous subsection. In this case, we discretise equations (38), (2) and (24) as:

$$\frac{u_{i,j+1} - u_{i,j}}{\Delta t} = \frac{1}{2}\left(G_{i,j} + G_{i,j+1}\right), \qquad i = \overline{0, M},\ j = \overline{0, (N-1)}, \tag{48}$$

$$u_{i,0} = \phi(x_i), \qquad i = \overline{0, M}, \tag{49}$$

$$u_{-1,j} - u_{1,j} = -2(\Delta x)\nu_1(t_j), \quad u_{M+1,j} - u_{M-1,j} = 2(\Delta x)\nu_2(t_j), \quad j = \overline{1, N}, \tag{50}$$

where $G_{i,j}$ is given by (40), and $u_{-1,j}$ and $u_{M+1,j}$ for $j = \overline{1, N}$ are fictitious values at points located outside the computational domain. Equations (48) can be rewritten in the form of the system (43) for $i = \overline{0, M}$, $j = \overline{0, (N-1)}$. At each time step $t_{j+1}$ for $j = \overline{0, (N-1)}$, using the Neumann boundary conditions (50), we obtain a $M \times M$ system of linear equations of the form,

$$\tilde{D}\tilde{\mathbf{u}}_{j+1} = \tilde{E}\tilde{\mathbf{u}}_j + \tilde{\mathbf{b}}, \tag{51}$$

where

$$\tilde{\mathbf{u}}_{j+1} = (u_{0,j+1}, u_{1,j+1}, ..., u_{M,j+1})^{tr},$$

$$\tilde{D} = \begin{pmatrix} 1 + B_{0,j+1} & -2C_{0,j+1} & 0 & \cdots & 0 \\ -C_{1,j+1} & & & & 0 \\ 0 & & D & & \vdots \\ \vdots & & & & -C_{M-1,j+1} \\ 0 & \cdots & 0 & -2C_{M,j+1} & 1 + B_{M,j+1} \end{pmatrix},$$

$$\tilde{E} = \begin{pmatrix} 1 - B_{0,j} & 2C_{0,j} & 0 & \cdots & 0 \\ C_{1,j} & & & & 0 \\ 0 & & E & & \vdots \\ \vdots & & & & C_{M-1,j} \\ 0 & \cdots & 0 & 2C_{M,j} & 1 - B_{M,j} \end{pmatrix},$$

and

$$\tilde{\mathbf{b}} = \begin{pmatrix} \frac{\Delta t}{2}(f_{0,j} + f_{0,j+1}) - 2(\Delta x)(C_{0,j}\nu_1(t_j) + C_{0,j+1}\nu_1(t_{j+1})) \\ \frac{\Delta t}{2}(f_{1,j} + f_{1,j+1}) \\ \vdots \\ \frac{\Delta t}{2}(f_{M-1,j} + f_{M-1,j+1}) \\ \frac{\Delta t}{2}(f_{M,j} + f_{M,j+1}) + 2(\Delta x)(C_{M,j}\nu_2(t_j) + C_{M,j+1}\nu_2(t_{j+1})) \end{pmatrix}.$$

In the above expressions the matrices $\tilde{D}$ and $\tilde{E}$ contain the matrices $D$ and $E$ of the Dirichlet direct problem defined in subsection 3.1.

### 3.2.1 Example

As an example, consider the direct problem (2), (6) and (24) with $T = L = 1$ and

$$\begin{aligned} a(t) = 1 + t, \quad b(x) = 2 - x^2, \quad \phi(x) = u(x,0) = x + \sin(x), \\ \nu_1(t) = -u_x(0,t) = -2, \quad \nu_2(t) = u_x(1,t) = 1 + \cos(1), \\ f(x,t) = 8 + (1+t)(2-x^2)\sin(x). \end{aligned}$$

The exact solution is given by (45) and the desired boundary temperature output (25) is

$$\mu_1(t) = u(0,t) = 8t. \tag{52}$$

The numerical and exact solutions for the temperature $u(x,t)$ at interior points are shown in Figure 3 and one can observe that an excellent agreement is obtained. Figure 4 shows excellent agreement between the numerical solution and the exact one for $\mu_1(t)$.

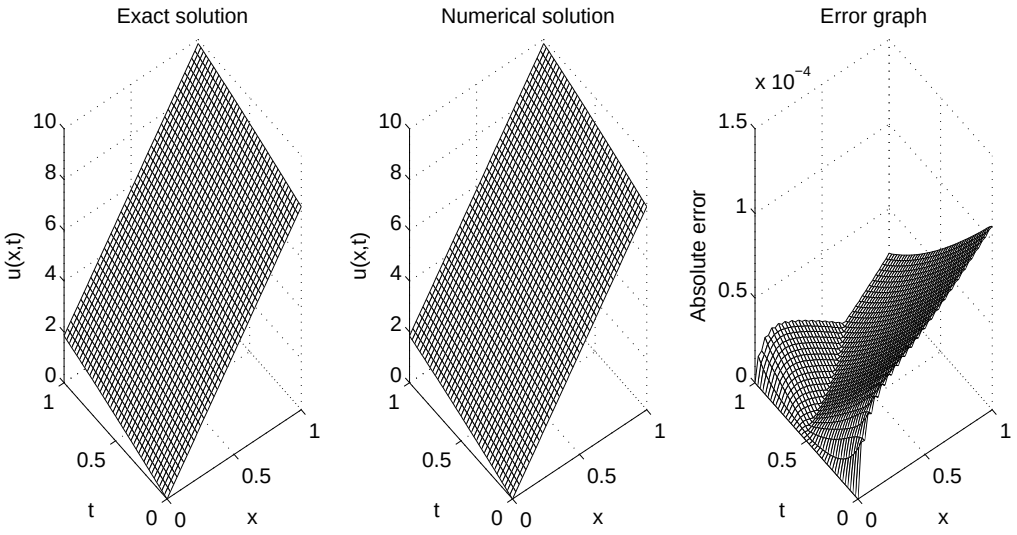


Figure 3: Exact and numerical solutions for the temperature $u(x,t)$ and the absolute error for the Neumann direct problem obtained with $M = N = 40$.

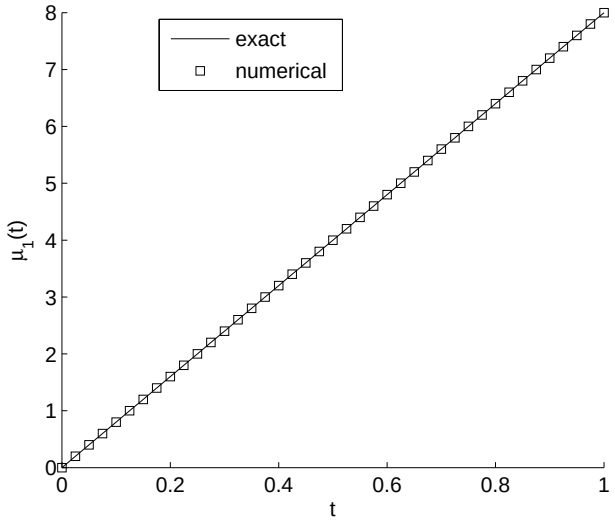


Figure 4: Exact and numerical solutions for $\mu_1(t)$ of the direct Neumann problem obtained with $M = N = 40$.

# 4 Solution of Inverse Problems

We wish to obtain stable and accurate reconstructions of the time-dependent thermal conductivity $a(t)$ and the temperature $u(x,t)$ satisfying the equations (2)–(4) and (6) for Inverse Problem I, and equations (2), (6), (24) and (25) for Inverse Problem II.

The most common approach based on imposing the measurement (4) or (25) in a least-squares sense, is minimizing

$$F_I(a) := \big\|a(t)u_x(0,t) + \mu_3(t)\big\|^2 + \beta\big\|a(t)\big\|^2, \tag{53}$$

for Inverse Problem I, and

$$F_{II}(a) := \big\|u(0,t) - \mu_1(t)\big\|^2 + \beta\big\|a(t)\big\|^2, \tag{54}$$

for Inverse Problem II, where $\beta \geq 0$ is a regularization parameter to be prescribed and the norm is usually the $L^2[0,T]$-norm. The discretization of (53) and (54) yields

$$F_I(\underline{a}) = \sum_{j=0}^{N} \Big[a_j u_x(0,t_j) + \mu_3(t_j)\Big]^2 + \beta \sum_{j=0}^{N} a_j^2, \tag{55}$$

$$F_{II}(\underline{a}) = \sum_{j=1}^{N} \Big[u(0,t_j) - \mu_1(t_j)\Big]^2 + \beta \sum_{j=0}^{N} a_j^2, \tag{56}$$

where $\underline{a} = (a_j)_{j=\overline{0,N}}$. It is worth mentioning that in (55) at the first time step, i.e. $j = 0$, the derivative $u_x(0,0)$ is obtained from the initial condition (2), via (47), as

$$u_x(0,0) = \frac{4\phi_1 - \phi_2 - 3\phi_0}{2(\Delta x)}, \tag{57}$$

where $\phi_i = \phi(x_i)$ for $i = \overline{0, M}$. Also, in (56), the value of $a(0)$ can be obtained by differentiating condition (25) with respect to $t$ and using equation (1) at $x = 0$, namely,

$$a(0) = \frac{\mu_1'(0) - f(0,0)}{b(0)\phi''(0)}. \tag{58}$$

The minimization of the objective function (55), or (56), subjected to the physical simple lower bound constraints $\underline{a} > \underline{0}$ is accomplished using the MATLAB toolbox routine *lsqnonlin*, which does not require supplying (by the user) the gradient of the objective function, [16].

This iterative routine attempts to solve a nonlinear least-squares minimization problem, starting from an initial guess, subject to constraints, and this generally is referred to as a constrained nonlinear optimization. We use the Trust-Region-Reflective (TRR) optimization algorithm from *lsqnonlin* [16] and the positive components of the vector $\underline{a}$ are sought in the interval ($10^{-10}$,$10^3$). The algorithm is based on the interior-reflective Newton method, [4, 5], and some details about how this is implemented for the minimization of a least-squares functional like (55), or (56), has recently been given in [10].

In the numerical implementation, we take the parameters of the routine *lsqnonlin* as follows:

- Number of variables $M = N = 40$.
- Maximum number of iterations = $10^2 \times$ (number of variables).
- Maximum number of objective function evaluations = $10^3 \times$ (number of variables).
- Solution Tolerance (aTol) = $10^{-20} \div 10^{-15}$.
- Object function Tolerance (FunTol) = $10^{-20} \div 10^{-15}$.
- Nonlinear constraint tolerance = $10^{-6}$.

The inverse problems under investigation are solved subjected to both exact and noisy heat flux measurement, (4) or (25) for Inverse Problems I and II, respectively. The noisy data is numerically simulated as

$$\mu_k^{\epsilon}(t_j) = \mu_k(t_j) + \epsilon_j^{(k)}, \quad j = \overline{0, N},\ k \in \{1, 3\}, \tag{59}$$

where $\epsilon_j$ are random variables generated from a Gaussian normal distribution with mean zero and standard deviation $\sigma_k$ given by

$$\sigma_k = p \times \max_{t \in [0,T]} |\mu_k(t)|, \quad k \in \{1, 3\}, \tag{60}$$

where $p$ represents the percentage of noise. We use the MATLAB function *normrnd* to generate the random variables $\underline{\epsilon}_k = \left(\epsilon_j^{(k)}\right)_{j=\overline{0,N}}$ as follows:

$$\underline{\epsilon}_k = normrnd(0, \sigma_k, N + 1). \tag{61}$$

The total amount of noise $\epsilon_k$ is given by

$$\epsilon_k = \left|\underline{\epsilon}_k\right| = \sqrt{\sum_{j=0}^{N} (\mu_k^{\epsilon}(t_j) - \mu_k(t_j))^2}, \quad k \in \{1, 3\}. \tag{62}$$

In the case of noisy data (59), we replace $\mu_3(t_j)$ by $\mu_3^{\epsilon}(t_j)$ for $j = \overline{0, N}$ in (55) and $\mu_1(t_j)$ by $\mu_1^{\epsilon}(t_j)$ for $j = \overline{1, N}$ in (56).

# 5 Numerical Results and Discussion

In this section, we present a few test examples to illustrate the accuracy and stability of the numerical scheme based on the FDM combined with the minimization of the least-squares functional (55), or (56), as described in Section 4. In order to explain the accuracy of the numerical results we introduce the root mean square error ($rmse$), defined as

$$rmse(a) = \sqrt{\frac{1}{N+1}\sum_{j=0}^{N}\left(a_{numerical}(t_j) - a_{exact}(t_j)\right)^2}. \tag{63}$$

We take $L = T = 1$ and present the numerical results obtained with $M = N = 40$. Unless otherwise specified, we take the initial guess as $\underline{a}^{(0)} = \underline{1}$.

## 5.1 Numerical Results for Inverse Problem I

We consider a couple of examples for the Inverse Problem I. Before we present the numerical results, we mention that regularization has not been found necessary and hence we consider $\beta = 0$ in the functional (55). Thus was to expected since, according to Theorem 3, the Inverse Problem I is stable in the $C[0,T]$ maximum norm with respect to small errors in the input data $\mu_3^{\epsilon}$.

### 5.1.1 Example 1

In this example, we consider the inverse problem (2)-(4) and (6) with the input data

$$\begin{aligned}
&\phi(x) = u(x,0) = x + \sin(x), \quad b(x) = 2 - x^2,\\
&\mu_1(t) = u(0,t) = 8t, \quad \mu_2(t) = u(1,t) = 1 + \sin(1) + 8t,\\
&f(x,t) = 8 + (1+t)(2-x^2)\sin(x), \quad \mu_3(t) = -a(t)u_x(0,t) = -2 - 2t.
\end{aligned}$$

One can observe that the conditions of Theorems 1 and 2 are satisfied hence the problem is uniquely solvable. The analytical solution is given by

$$a(t) = 1 + t, \quad u(x,t) = x + \sin(x) + 8t. \tag{64}$$

We start with the case of exact input data, i.e. there is no noise included in (4). Figure 5 represents the objective functional (55), as a function of the number of iterations. From this figure it can be seen that the decreasing convergence is very fast and is achieved in 10 iterations to reach a stationary value of $O(10^{-24})$. In fact, the objective function reaches this plateau immediately after only four iterations. The numerical results for the time-dependent thermal conductivity $a(t)$ are depicted in Figure 6. From this figure it can be seen that the agreement between the numerical (final iteration 10) and exact solutions for $a(t)$ is excellent. Also, the $rmse$ values versus the number of iterations are shown in Figure 7. From this figure it can be easily remarked that the $rmse(a)$ quickly decreases in the first two iterations after which it becomes stationary at a very low value of 0.0002.

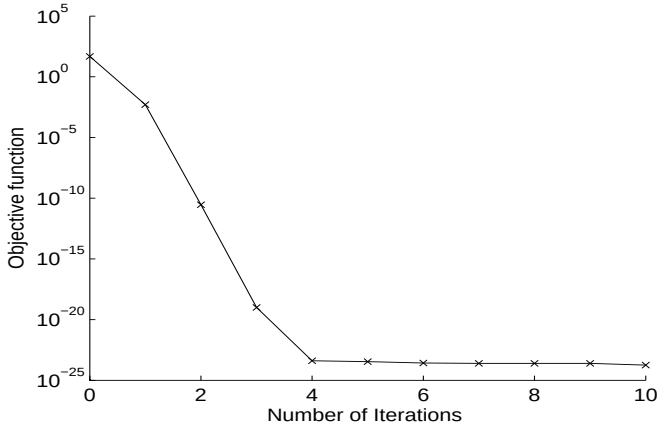


Figure 5: The objective function (55), for Example 1 with no noise.

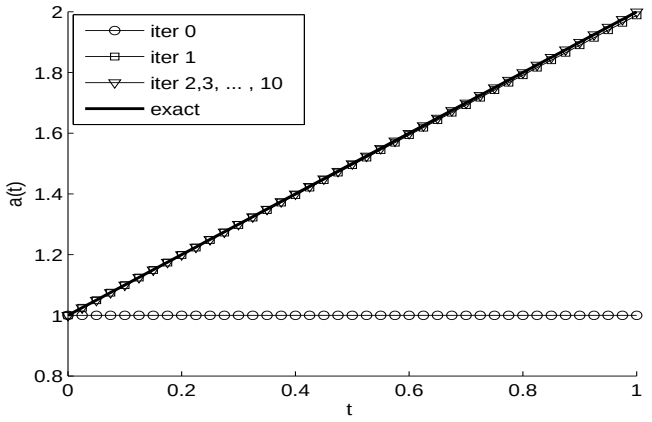


Figure 6: The thermal conductivity $a(t)$, for Example 1 with no noise.

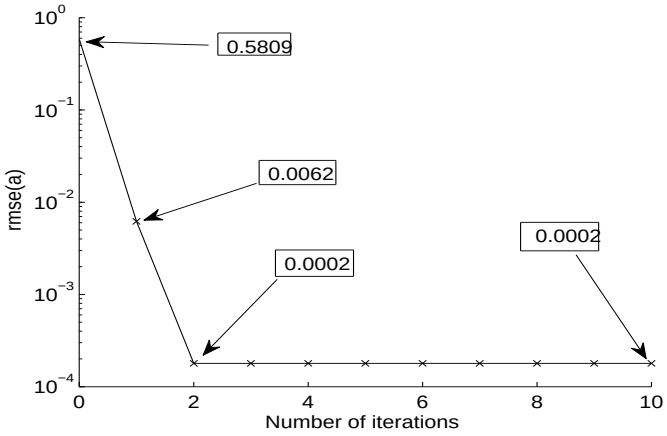


Figure 7: The *rmse* values of $a(t)$, versus the number of iterations, for Example 1 with no noise.

Next, we investigate the stability of the numerical solution with respect to noise in the data (4), defined by equation (59). We include $p \in \{2\%, 20\%\}$ noise and then, the

total amount of noise that is applied is $\epsilon_3 \in \{0.3540, 3.5392\}$, respectively, as defined by equation (62). Figure 8 represents the exact $\mu_3(t)$ and a typical noisy measurement input data $\mu_3^\epsilon(t)$.

Figure 9 represents the objective functional (55), as a function of number of iterations, when $p \in \{2\%, 20\%\}$. From this figure it can be seen that a very fast decreasing convergence is achieved for $p \in \{2\%, 20\%\}$ in 8 iterations each, to reach a stationary value of $O(10^{-24})$.

Figures 10–12 show the numerical solutions for the thermal conductivity $a(t)$, the heat flux $a(t)u_x(1,t)$ at $x = 1$, and the $rmse(a)$ values, respectively, for $p \in \{2\%, 20\%\}$ noise. From these figures, as well as Figure 6, it can be seen that the numerical solution for the thermal conductivity $a(t)$ converges to the exact solution $a(t) = 1 + t$, as the percentage of noise $p$ decreases from 20% to 2% and then to 0. The nonlinear least-squares minimization produces good and consistent retrievals of the solution even for a large amount of noise such as 20%. In Figure 12, for $p = 20\%$ a slight 'semi-convergence' phenomenon seems to appear after a couple of iterations, but this is more likely to be attributed to a non-monotonic decreasing convergence rather than to the former phenomenon which is commonly encountered when solving ill-posed problems iteratively, [8]. That is to say, our inverse problem is rather stable and in fact, as mentioned before at the beginning of Section 5.1, no regularization was needed to be included in the least-squares functional (55).

Finally, Figure 13 shows the exact solution, the numerical solution for the temperature $u(x,t)$ and the relative error between them. From this figure it can be seen that the numerical solution is stable and furthermore, its accuracy is consistent with the amount of noise shown in Figure 8, which was included into the input data (4).

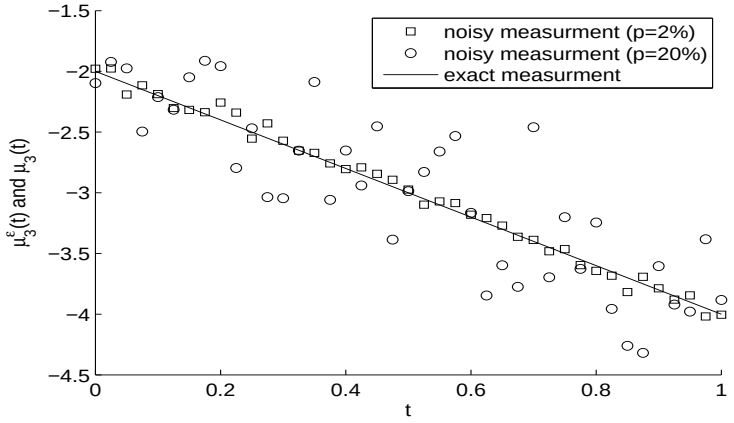


Figure 8: The noisy $\mu_3^\epsilon(t)$ and exact $\mu_3(t)$, for Example 1 with $p \in \{2\%, 20\%\}$ noise.

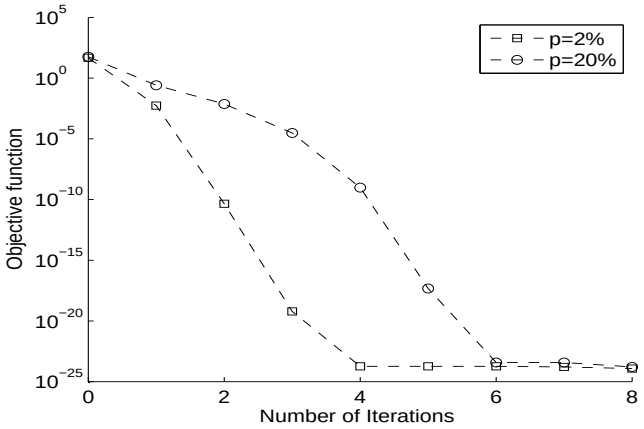


Figure 9: The objective function (55), for Example 1 with $p \in \{2\%, 20\%\}$ noise.

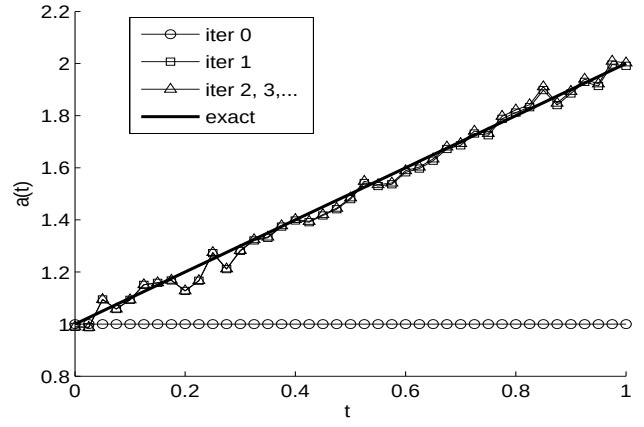


(a)

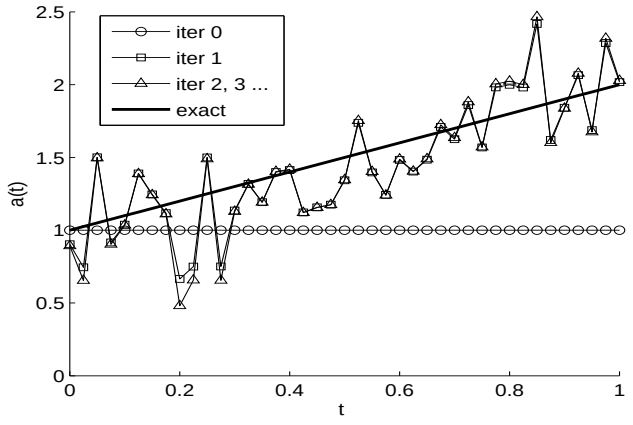


(b)

Figure 10: The thermal conductivity $a(t)$, for Example 1 with (a) $p = 2\%$ and (b) $p = 20\%$ noise.

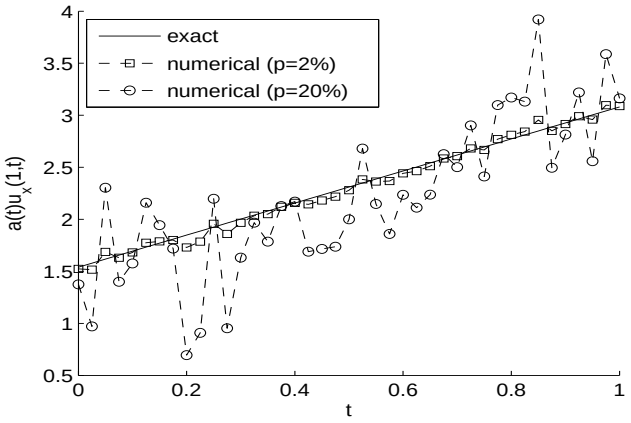


Figure 11: The exact and numerical heat flux $a(t)u_x(1,t)$, for Example 1 with $p \in \{2\%, 20\%\}$ noise.

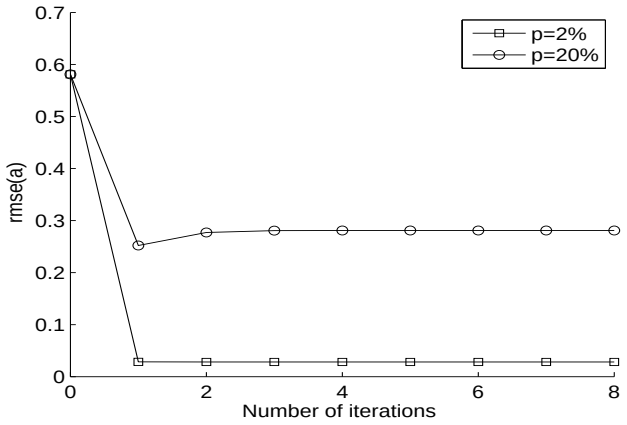


Figure 12: The *rmse* values of $a(t)$, versus the number of iterations, for Example 1 with $p \in \{2\%, 20\%\}$ noise.

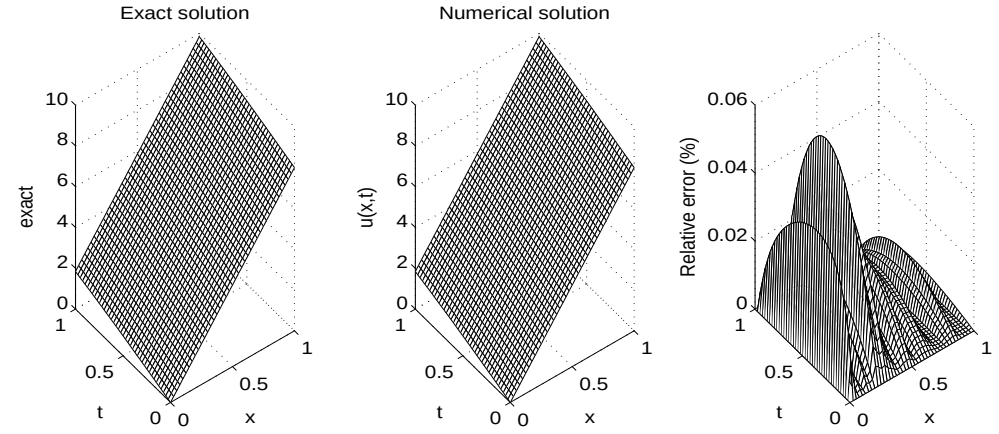


(a)

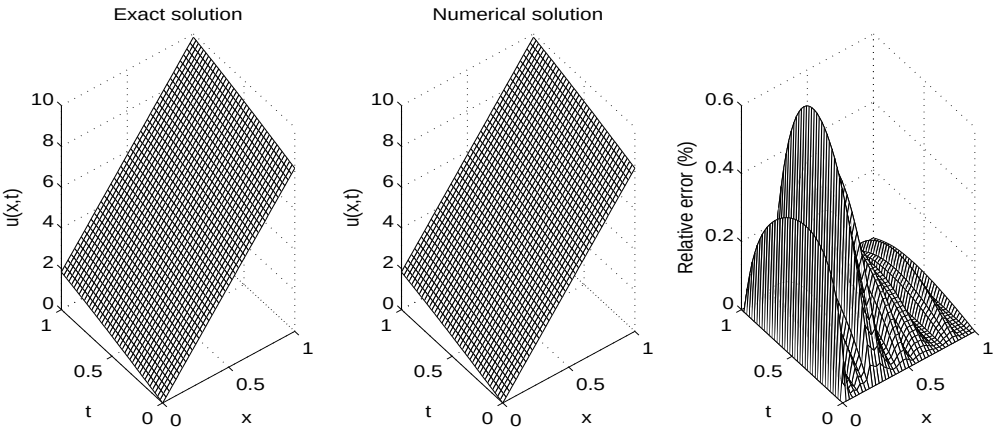


(b)

Figure 13: The exact and numerical temperature $u(x,t)$, for Example 1 with (a) $p = 2\%$ and (b) $p = 20\%$ noise. The relative error between them is also included.

### 5.1.2 Example 2

In the previous example we have inverted the unknown thermal conductivity $a(t) = 1 + t$ which is a smooth function. In this example, we consider a non-smooth test function, see equation (65). We consider the inverse problem (2)–(4) and (6) with the following input data

$$\begin{aligned}\phi(x) =& u(x,0) = xe^x, \quad b(x) = 2 - x^2, \quad \mu_1(t) = u(0,t) = t^2,\\ &\mu_2(t) = u(1,t) = e + t^2, \quad \mu_3(t) = -a(t)u_x(0,t) = -1 - \left|t - \frac{1}{2}\right|,\\ &f(x,t) = 2t - \left(1 + \left|t - \frac{1}{2}\right|\right)(2 - x^2)(xe^x + 2e^x).\end{aligned}$$

One can notice that the conditions of Theorem 2 are satisfied hence the uniqueness of the solution holds. With this data, the analytical solution of the Inverse Problem I is given by

$$a(t) = 1 + \left|t - \frac{1}{2}\right|, \quad u(x,t) = xe^x + t^2. \tag{65}$$

We study the case of exact and noisy input data (4). The objective function (55), as a function of the number of iterations, is presented in Figure 14. Form this figure it can be seen that the same fast decreasing convergence is achieved as in Example 1.

The numerical results for the corresponding time-dependent thermal conductivity $a(t)$, the heat flux $a(t)u_x(1,t)$, the $rmse(a)$ values and the interior temperature $u(x,t)$ are presented in Figures 15–18, respectively. The same conclusions as those obtained for Example 1 can be drawn by observing these figures.

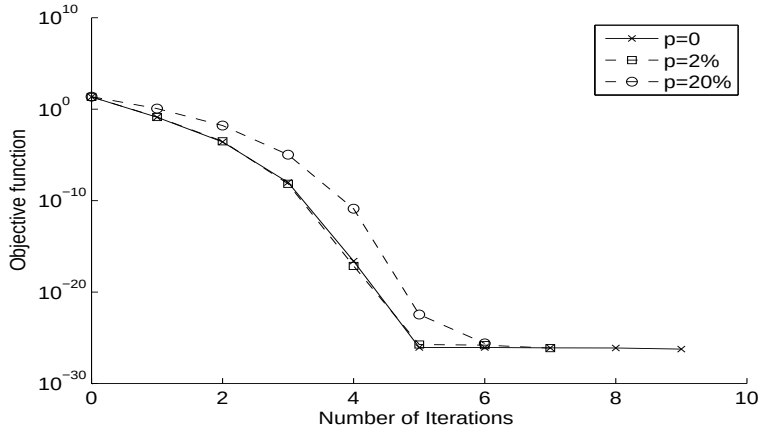


Figure 14: The objective function (55), for Example 2 with $p \in \{0, 2\%, 20\%\}$ noise.

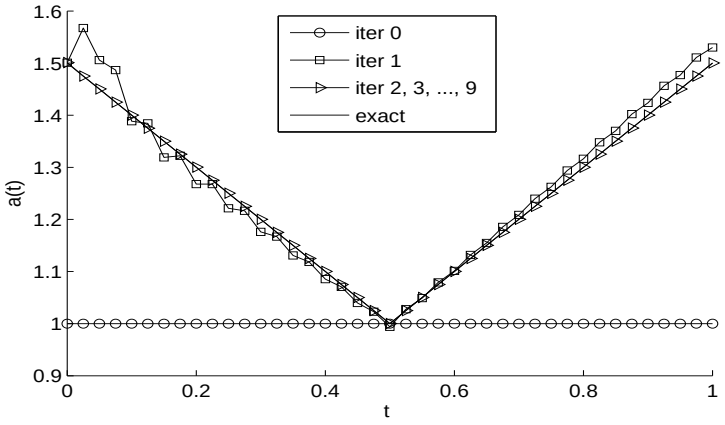


(a)

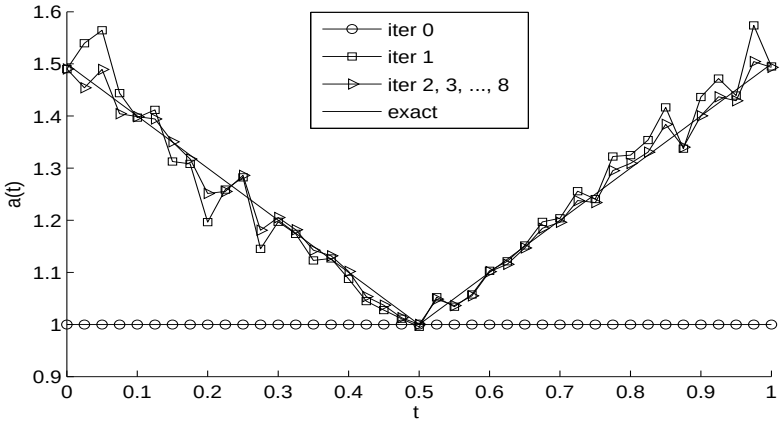


(b)

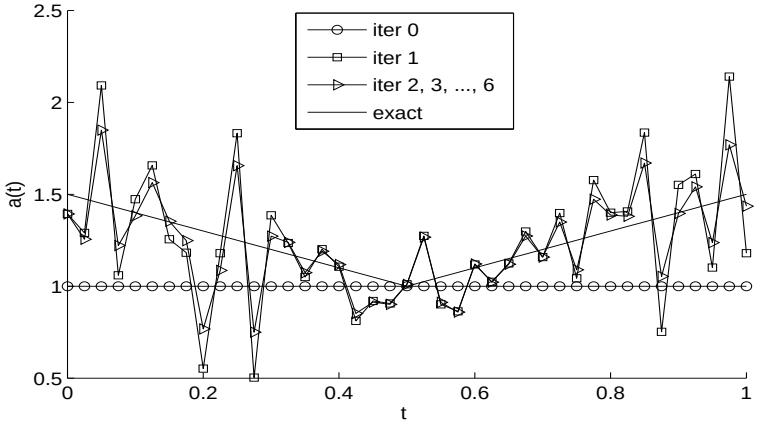


(c)

Figure 15: The thermal conductivity $a(t)$, for Example 2 with (a) $p = 0$, (b) $p = 2\%$ and (c) $p = 20\%$.

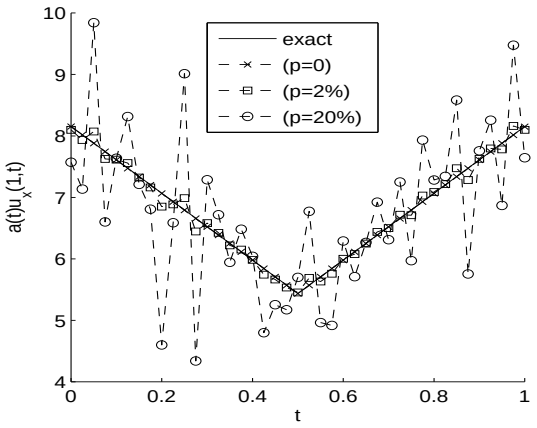


Figure 16: The exact and numerical heat flux $a(t)u_x(1,t)$, for Example 2 with $p \in \{0, 2\%, 20\%\}$ noise.

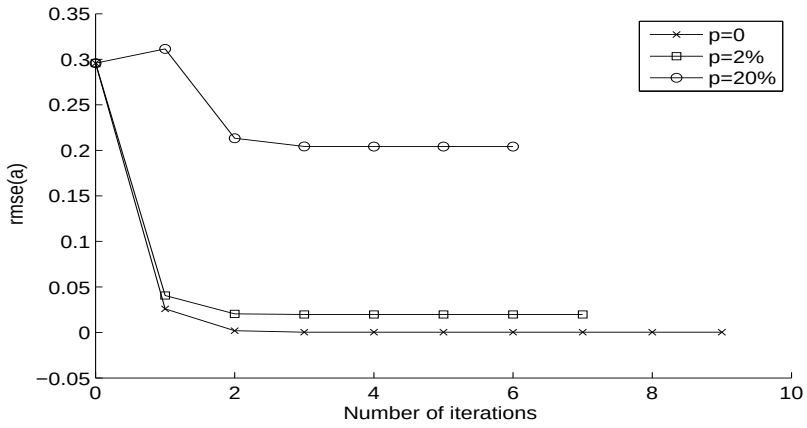


Figure 17: The *rmse* values of $a(t)$, versus the number of iterations, for Example 2 with $p \in \{0, 2\%, 20\%\}$ noise.

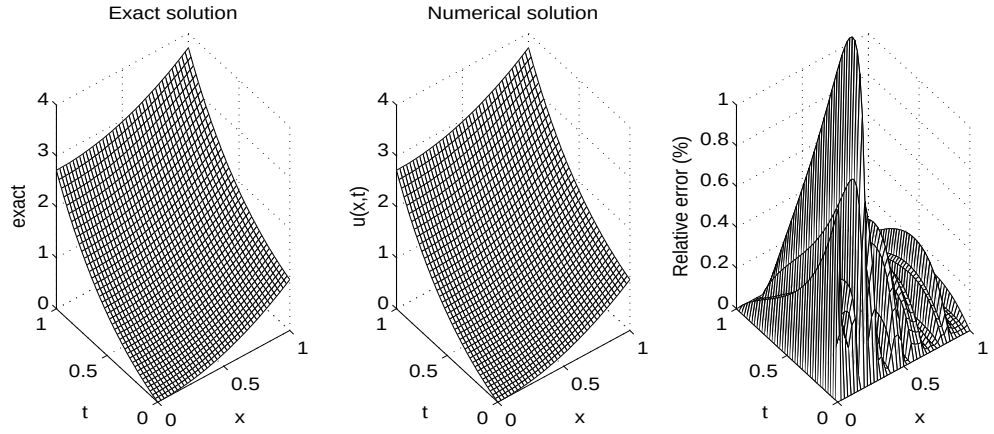


(a)

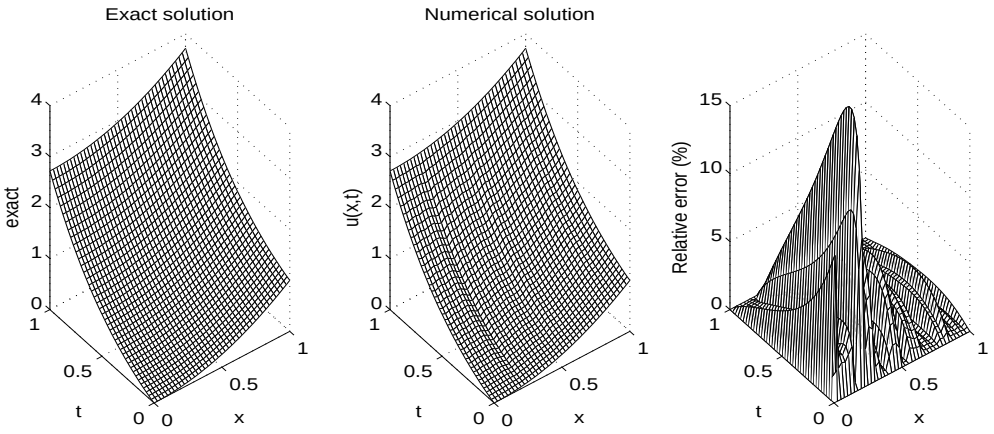


(b)

Figure 18: The exact and numerical temperature $u(x,t)$, for Example 2 with (a) $p = 2\%$ and (b) $p = 20\%$ noise. The relative error between them is also included.

Numerical outputs such as the number of iterations and function evaluations, as well as the final value of the convergent objective function are provided in Table 1 for both Examples 1 and 2.

Table 1: Number of iterations, number of function evaluations, value of objective function (55) at final iteration, for Examples 1 and 2 with $p \in \{0, 2\%, 20\%\}$ noise.

| Example | Numerical outputs | $p = 0$ | $p = 2\%$ | $p = 20\%$ |
|---|---|---|---|---|
| 1 | No. of iterations | 10 | 8 | 8 |
| | No. of function evaluations | 451 | 328 | 328 |
| | Function value | $1.7E-24$ | $1.1E-24$ | $1.6E-24$ |
| | $rmse(a)$ | $1.7E-4$ | 0.0282 | 0.2809 |
| 2 | No. of iterations | 9 | 7 | 6 |
| | No. of function evaluations | 369 | 287 | 246 |
| | Function value | $5.8E-27$ | $7.4E-27$ | $2.8E-26$ |
| | $rmse(a)$ | $2.6E-4$ | 0.0197 | 0.2041 |

## 5.2 Numerical Results for Inverse Problem II

We now consider a couple of examples for the Inverse Problem II. Unlike for the Inverse Problem I which has been found stable with respect to noise in the input data (4), for the Inverse Problem II regularization was found necessary to be included in the functional (56) in order to obtain stable numerical solutions. This is to be expected since in the stability estimate (26) of Theorem 6, the right-hand side term contains the noisy data $(\mu_1^\epsilon - \mu_1)$ in the $C^1[0,T]$-norm which where differentiated produce an unstable numerical solution.

### 5.2.1 Example 3

In this example, we consider the inverse problem (2), (6), (24) and (25) with the input data

$$\begin{aligned} \phi(x) = u(x,0) = 1 + xe^x, \quad b(x) = 2 - x^2, \\ \nu_1(t) = -u_x(0,t) = -1, \quad \nu_2(t) = u_x(1,t) = -2e, \\ f(x,t) = e^t - (1+t)(2-x^2)(xe^x + 2e^x), \quad \mu_1(t) = u(0,t) = e^t. \end{aligned}$$

One can observe that the conditions of Theorem 5 are satisfied hence, a solution is unique. The analytical solution is given by

$$a(t) = 1 + t, \quad u(x,t) = xe^x + e^t. \tag{66}$$

We start the investigation with exact input data (25), i.e. there is no noise included. Figure 19 represents the evolution of objective functional (56), as a function of the number of iterations, with no regularization, i.e. $\beta = 0$. From this figure it can be seen that a fast decreasing convergence is achieved in 7 iterations to reach a very low value of order $O(10^{-26})$. The corresponding numerical results of the time-dependent thermal conductivity $a(t)$ are displayed in Figure 20. From this figure it can be seen that there is an excellent agreement between the exact and numerical solutions with an $rmse(a)$= 0.0086.

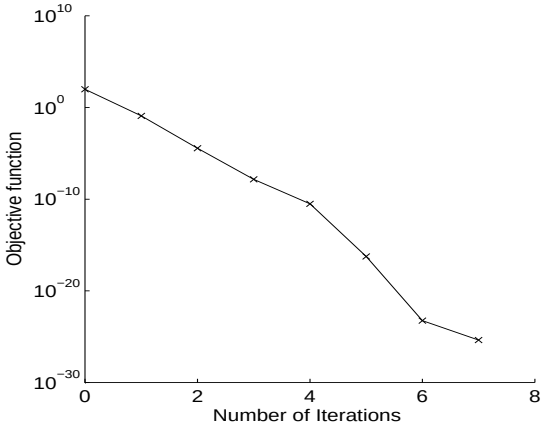


Figure 19: The objective function (56), for Example 3 with no noise and no regularization.

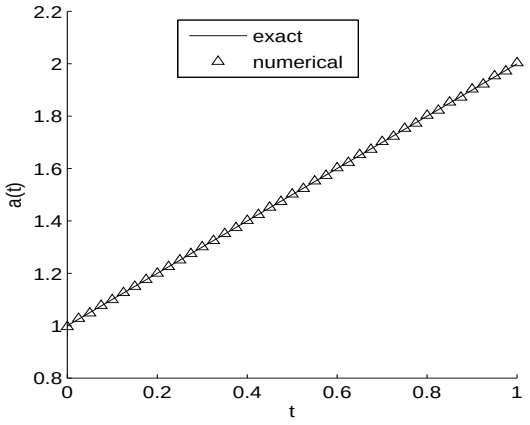


Figure 20: The thermal conductivity $a(t)$, for Example 3 with no noise and no regularization.

In order to test the stability of the problem, we add $p = 2\%$ random Gaussian additive noise as in (59) which, according to (62), yields the total amount of noise $\epsilon_1 = 0.2314$. Let us denote by

$$R_{II}(\underline{a}) = \sum_{j=1}^{N} [u(0, t_j) - \mu_1^{\epsilon}(t_j)]^2, \tag{67}$$

the least-squares residual associated to the regularized Tikhonov functional (56).

Figure 21 shows the residual functional (67), as a function of the number of iterations, for various regularization parameters $\beta \in \{0, 10^{-3}, 10^{-2}, 10^{-1}\}$. From this figure one can observe that convergence is rapidly achieved for each value of $\beta$. The resulting thermal conductivity is plotted in Figure 22 for various regularization parameters. As expected, when no regularization is employed, i.e. $\beta = 0$, the estimated $a(t)$ is highly unstable and inaccurate. This shows that the Inverse Problem II is ill-posed. Consequently, a small perturbation in input data (25) causes a drastic error in the output solution $a(t)$. In order to overcome this instability, we employ the Tikhonov regularization method with $\beta > 0$. From Figure 22 and Table 2, it can be observed that the stability is indeed restored and the value of $\beta = O(10^{-2})$ produces the most accurate numerical results.

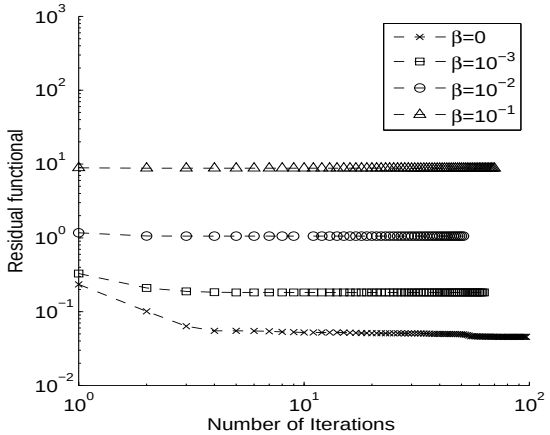


Figure 21: The residual function (67), for Example 3 with $p = 2\%$ noise, and various regularization parameters.

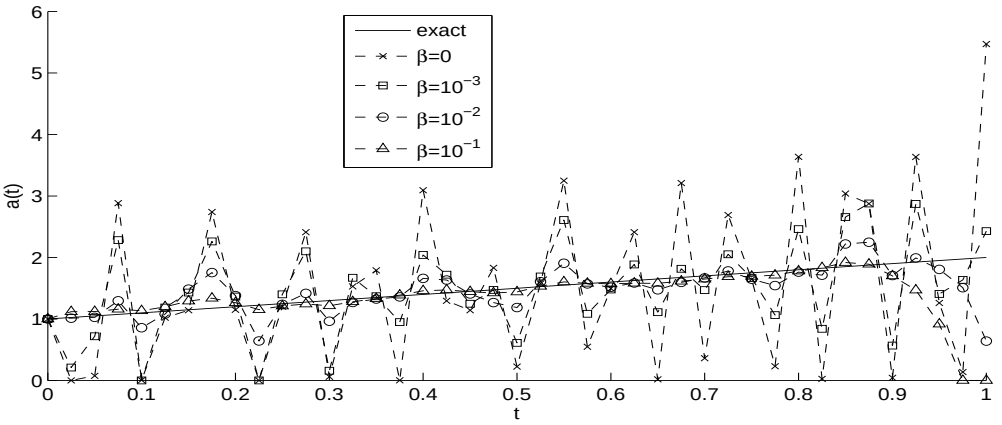


Figure 22: The thermal conductivity $a(t)$, for Example 3 with $p = 2\%$ noise and various regularization parameters.

Finally, Figure 23 shows the exact solution, the numerical solution for the temperature $u(x,t)$ and the relative error between them. From this figure it can be seen that the numerical solution for $u(x,t)$ is stable for all values of $\beta$ with only very small instabilities manifesting for $\beta = 0$ or $10^{-3}$.

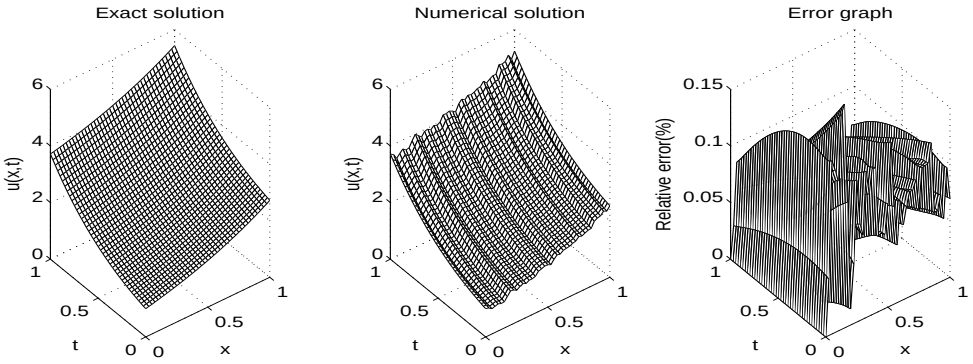


(a)

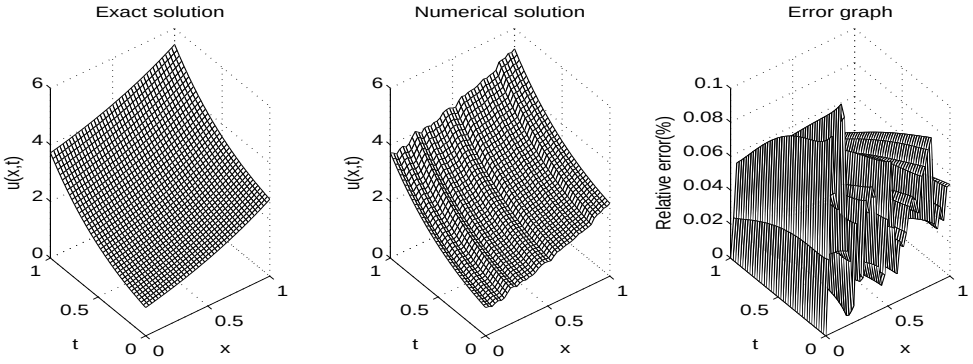


(b)

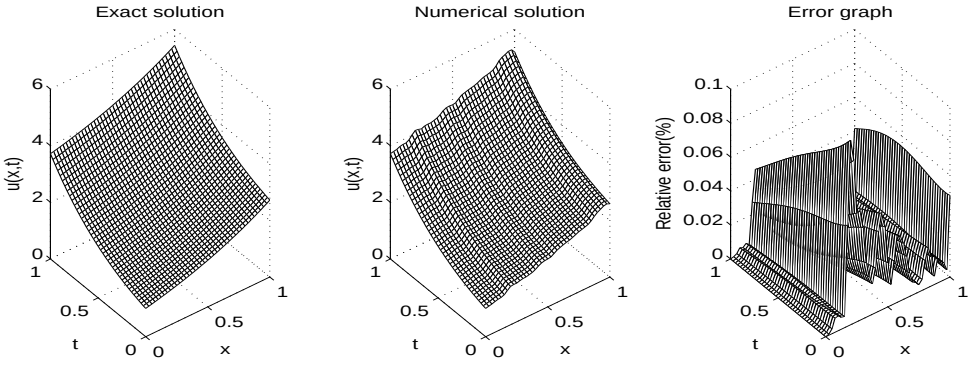


(c)

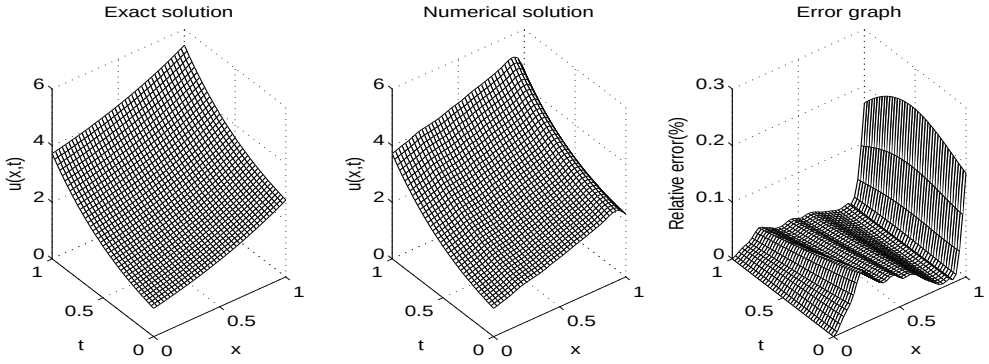


(d)

Figure 23: The exact and numerical temperature $u(x,t)$, for Example 1 with $p = 2\%$ noise and (a) $\beta = 0$, (b) $\beta = 10^{-3}$, (c) $\beta = 10^{-2}$, and (d) $\beta = 10^{-1}$. The relative error between them is also included.

### 5.2.2 Example 4

Consider the inverse problem (2), (6), (24) and (25) with the input data

$$\begin{aligned}
&\phi(x) = u(x,0) = e^x, \quad b(x) = 2 - x^2, \\
&\nu_1(t) = -u_x(0,t) = -e^t, \quad \nu_2(t) = u_x(1,t) = e^{1+t}, \\
&f(x,t) = e^{x+t} - (1 + 2\pi\cos(2\pi t)^2)(2 - x^2)e^{x+t}, \quad \mu_1(t) = u(0,t) = e^t.
\end{aligned}$$

The analytical solution is given by

$$a(t) = 1 + 2\pi\cos^2(2\pi t), \quad u(x,t) = e^{x+t}. \tag{68}$$

For this thermal conductivity the initial guess was $\underline{a_0} = \underline{1 + 2\pi}$. The objective function (56), as a function of the number of iterations, is depicted in Figure 24 for no noise and no regularization. From this figure it can be seen that the objective function (56) with $\beta = 0$, i.e the residual functional (67), is decreasing over several orders of magnitude, as the number of iterations increases, reaching a very low value of $O(10^{-15})$ after 400 iterations. The computational time taken by the *lsqnonlin* to produce this convergence was about 10.6 minutes. The resulting thermal conductivity is shown in Figure 25 and very good agreement between the exact and numerical solutions can be observed.

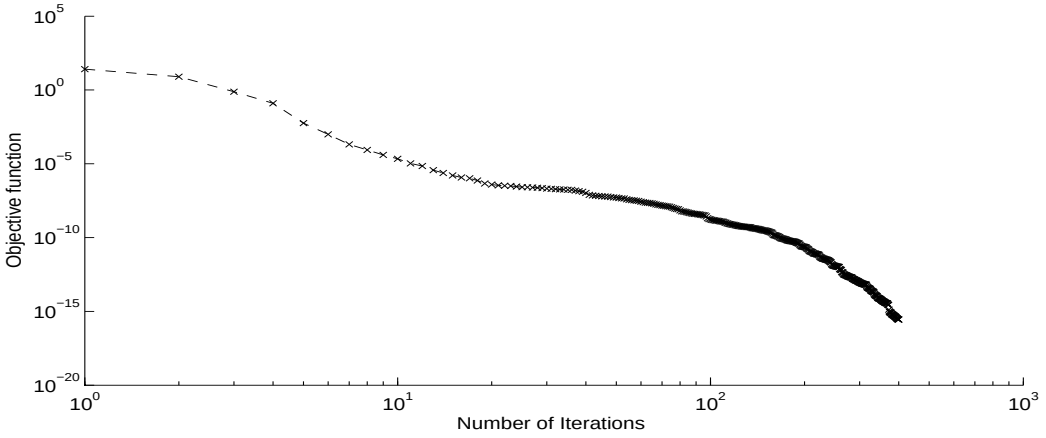


Figure 24: The objective function (56), for Example 4 with no noise and no regularization.

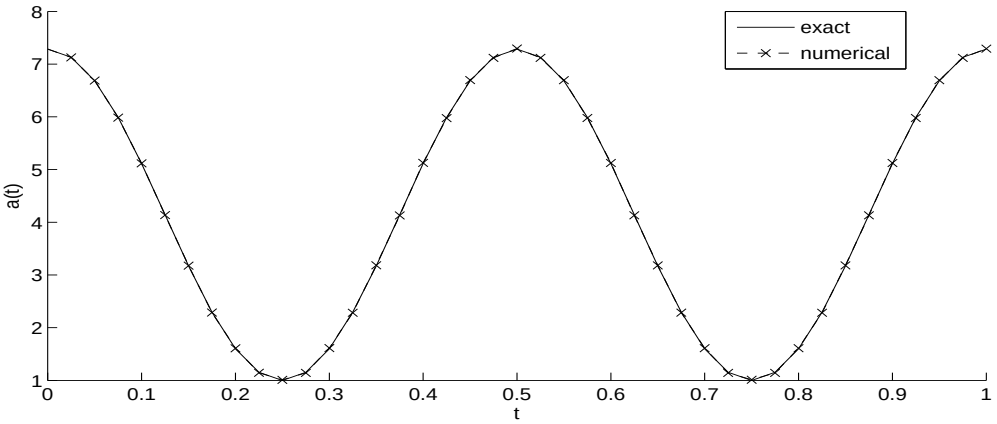


Figure 25: The thermal conductivity $a(t)$, for Example 3 with no noise and no regularization.

Next, the input data (25) was perturbed by $p = 2\%$ noise. The residual function (67), as a function of the number of iterations, and the numerical results for $a(t)$ are plotted in Figures 26 and 27, respectively, for various regularization parameters $\beta \in \{0, 10^{-3}, 10^{-2}, 10^{-1}\}$. As in Example 3, one can see that the numerically obtained results for $\beta = 0$ in Figure 27 are unstable being highly oscillatory and unbounded. However, the inclusion of some regularization with $\beta > 0$ in the objective functional (56) restores the stability of the numerical solution, as shown further in Figure 27. One can observe that the choice $\beta = 10^{-1}$ is too large and it oversmooths the solution, whilst the choice $\beta = 10^{-3}$ is too small and it undersmooths the solution. It seems that a regularization parameter $\beta$ of $O(10^{-2})$ realizes the desired compromise of balancing the under- and over-smooth regions. Finally, Figure 27, as well as Figure 22 for Example 3, give some insight about how one may choose the regularization parameters $\beta > 0$. Based on practical experience, on can start with a rather large values for $\beta$, and then decrease it until oscillations in the numerical solution start to appear [7].

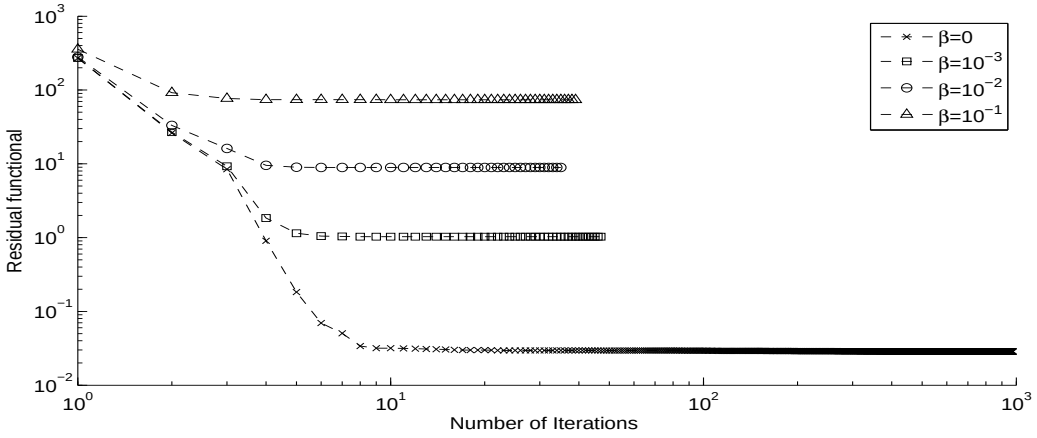


Figure 26: The residual function (67), for Example 4 with $p = 2\%$ noise and various regularization parameters.

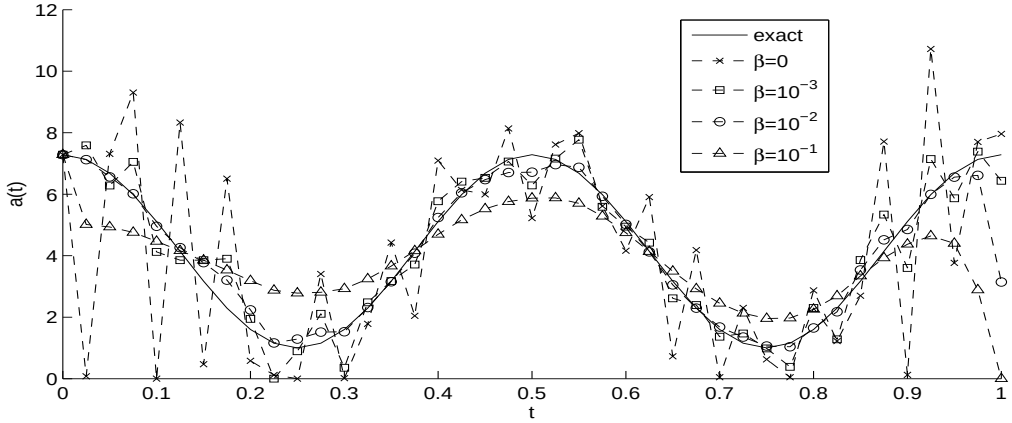


Figure 27: The thermal conductivity $a(t)$, for Example 4, with $p = 2\%$ noise and various regularization parameters.

For completeness, numerical outputs such as the number of iterations and function

evaluations, the final value of the convergent objective function, as well as the $rmse(a)$ are provided in Table 2 for Examples 3 and 4.

The numerical results for the temperature $u(x,t)$ were found, as in Figure 23 for Example 3, accurate and stable and therefore they are not presented. Finally, although not illustrated, it is reported that an accurate and stable retrieval also was obtained for a non-smooth thermal conductivity.

Table 2: Number of iterations, number of function evaluations, value of regularized objective function (56) at final iteration, and the $rmse(a)$ for Examples 3 and 4 with $\beta \in \{0, 10^{-3}, 10^{-2}, 10^{-1}\}$ and $p = 2\%$ noise.

| Example | Numerical outputs | $\beta = 0$ | $\beta = 10^{-3}$ | $\beta = 10^{-2}$ | $\beta = 10^{-1}$ |
|---|---|---|---|---|---|
| 3 | No. of iterations | 97 | 63 | 51 | 70 |
| | No. of function evaluations | 4116 | 2688 | 2184 | 2982 |
| | Function value | 0.0455 | 0.1818 | 1.0574 | 8.7697 |
| | $rmse(a)$ | 1.2697 | 0.6829 | 0.3158 | 0.4836 |
| 4 | No. of iterations | 976 | 49 | 41 | 42 |
| | No. of function evaluations | 40016 | 2016 | 1764 | 1806 |
| | Function value | 0.0286 | 1.029 | 8.917 | 73.817 |
| | $rmse(a)$ | 2.4973 | 0.7479 | 0.7135 | 1.7179 |

# 6 Conclusions

A couple of inverse problems which require determining a time-dependent thermal conductivity when the spacewise dependent heat capacity is given for the heat parabolic equation under overspecified conditions have been investigated. The Inverse Problem I given by equations (2)–(4) and (6) was found to be well-posed, whilst the Inverse Problem II given by equations (2), (6), (24) and (25) was found to be ill-posed and needed regularization in order to obtain a stable solution. A direct solver based on a Crank-Nicolson finite difference scheme has been developed. The inverse solver is based on a nonlinear least-squares minimization which has been solved numerically using the MATLAB toolbox routine *lsqnonlin*. Numerical results illustrated for several benchmarks test examples show that an accurate and stable solution has been obtained.

Future work will consider extending the present study to the simultaneous identification of several time-dependent parameters in the reaction-diffusion-convection equation, [12].

**Acknowledgments.** M.S. Hussein would like to thank the Higher Committee of Education Development in Iraq (HCEDiraq) for their financial support in this research. The authors would like to thank Professor M. Ivanchov for discussions on the topic of this work.

# References

[1] Cannon, J.R. (1984) *The One-Dimensional Heat Equation*, Encyclopedia of Mathematics and its Applications, Vol. 23, Addison-Wesley Publishing Company, Menlo

Park, California.

[2] Cannon, J.R. and DuChateau, P. (1973) Determining unknown coefficients in a nonlinear heat conduction problem, *SIAM Journal on Applied Mathematics*, **24**, 298–314.

[3] Cannon, J.R. and Rundell, W. (1991) Recovering a time-dependent coefficient in a parabolic differential equation, *Journal of Mathematical Anaysis and Applications*, **160**, 572–582.

[4] Coleman, T.F. and Li, Y. (1994) On the convergence of interior-reflective Newton methods for nonlinear minimization subject to bounds, *Mathematical Programming*, **67**, 189–224.

[5] Coleman, T.F. and Li, Y. (1996) An interior trust, region approach for nonlinear minimization subject to bounds, *SIAM Journal on Optimization*, **6**, 418–445.

[6] Doris, H.G., Peralta, J. and Luis, E.O. (2013) Regularization algorithm within two parameters for the identification of the heat conduction coefficient in the parabolic equation, *Mathematical and Computer Modelling*, **57**, 1990–1998.

[7] Dennis, B.H., Dulikravich, G.S. and Yoshimura, S. (2004) A finite element formulation for the determination of unknown boundary conditions for three-dimensional steady thermoelastic problems, *Journal of Heat Transfer*, **126**, 110–118.

[8] Elfving, T., Nikazad, T. and Hansen, P.C. (2010) Semi-convergence and relaxation parameters for a class of SIRT algorithms, *Electronic Transactions on Numerical Analysis*, **37**, 321–336.

[9] Ismailov, M.I. and Kanca, F. (2012) The inverse problem of finding the time-dependent diffusion coefficient of the heat equation from integral overdetermination data, *Inverse Problems in Science and Engineering*, **20**, 463-476.

[10] Ito, K. and Liu, J.-C. (2013) Recovery of inclusions in 2D and 3D domains for Poisson's equation, *Inverse Problems*, **29**, 075005 (20 pages).

[11] Ivanchov, M.I. (1997) Inverse problem of finding a major coefficients in a parabolic equation, *Matematychni Studii*, **8**, 212–220.

[12] Ivanchov, M.I. (2000) Inverse problem of simultaneous determination of two coefficients in a parabolic equation, *Ukrainian Mathematical Journal*, **52**, 379–387.

[13] Ivanchov, M.I. (2003) *Inverse Problems for Equations of Parabolic Type*, VNTL Publications, Lviv, Ukraine.

[14] Lesnic, D., Yousefi, S.A. and Ivanchov, M. (2013) Determination of a time-dependent diffusivity from nonlocal conditions, *Journal of Applied Mathematics and Computing*, **41**, 301–320.

[15] Smith, G.D. (1985) *Numerical Solution of Partial Differential Equations: Finite Difference Methods*, Oxford Applied Mathematics and Computing Science Series, Third Edition.

[16] Mathworks R2012 Documentation Optimization Toolbox-Least Squares (Model Fitting) Algorithms, available from www.mathworks.com/help/toolbox/optim/ug /brnoybu.html.

[17] Wang, Y., Yang, C. and Yagola, A. (2011) *Optimization and Regularization for Computational Inverse Problems and Applications*, Springer-Verlag, Berlin.

[18] Wang, P. and Zheng, K. (2002) Determination of an unknown coefficient in a nonlinear heat equation, *Journal of Mathematical Analysis and Applications*, **271**, 525–533.

[19] Yousefi, S.A., Lesnic, D. and Barikbin, K. (2012) Satisfier function in Ritz-Galarkin method for the identification of a time-dependent diffusivity, *Journal of Inverse and Ill-Posed Problems*, **20**, 701–722.